”Enhancing digital measurement bandwidth through novel frequency folding technique”

Sjouke Spijkerman, ir. Patrick D. Koch*, dr. ir. Tom H.F. Hartman**, dr. ir. Ronan A.R. van der zee***
*Daily supervisor, **Assistant professor, ***External committee member
BSc Thesis Electrical Engineering, University of Twente, Faculty of EEMCS
June 20, 2023

***Abstract*—In this paper, a novel new way of increasing bandwidth for digital measuring is presented. In previous work, bandwidth is increased by increasing the sampling rate, using several samplers, or sampling more frequently. For this new approach, a custom passive LC filter structure consisting of 3 filters is designed and verified by simulation, which in a controlled manner allows for frequencies to fold over the Nyquist frequency. Results show that these filters in combination with digital signal processing realises tripling of the bandwidth for mono-frequency signals. However, for multi-frequency signals, unambiguous frequencies are not guaranteed. This is due to aliasing in the transition areas of filters of frequencies from transition bands into the initially intended pass-band of the filter.**

***Index Terms*—Measurement systems, bandwidth enlargement, Aliasing.**

I. Introduction

Modern-day digital oscilloscopes use to have an Anti-Aliasing Filter (AAF). An AAF attenuates frequencies above the Nyquist frequency in order to prevent signals from folding into the bandwidth of an oscilloscope. This bandwidth will be called the baseband from this point onwards. This way only one frequency can be expected to occur on a specific frequency in the baseband. Doing this ensures that the frequency components of a signal measured by an oscilloscope are determinable and not ambiguous.

Although this solves aliasing, it discards a great amount of the bandwidth of a possible input signal. To increase the bandwidth, one could increase the sampling frequency. This creates a higher Nyquist frequency and thus increased bandwidth. Another approach is a method such as time dithering [1]. This approach is based on sampling a signal several times instead of once while adding a random delay every time another run of sampling is performed. One could also use two samplers with a different sampling rate at the same time [2]. This results in two different Nyquist frequencies which allow for frequencies to fold to different spots into the baseband of the oscilloscope. By combining this with signal processing, the bandwidth can be expanded. In this paper, another novel approach has been proposed for increasing the bandwidth of a frequency-measuring device, which is based on the folding of frequencies after the Nyquist frequency.

Some low-end oscilloscopes lack an AAF [3]. An input/output frequency measurement for a low-end oscilloscope with a bandwidth of 20MHz is performed, which can be seen in fig.1. Firstly, this measurement shows that frequencies after the Nyquist frequency mirror into the baseband of the oscilloscope until twice the Nyquist frequency at 40MHz. After this frequency, the output frequency starts to increase again until 60MHz after which frequencies restart to fold in a mirror-fashioned.

Using this fact, one could make a parallel filter structure,

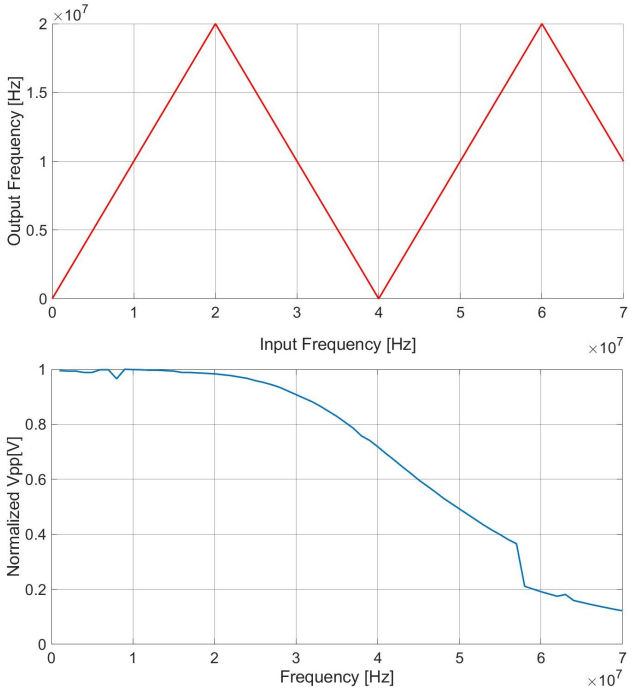

Fig. 1. Frequency and magnitude response of low-end oscilloscope

which only passes frequencies for:

$$n * f_{Nyquist} \leq f \leq (n+1) * f_{Nyquist} \tag{1}$$

for which n is an integer.

This way, frequencies from above the Nyquist frequency can fold and not become ambiguous, since only one frequency can occur on one frequency in the baseband of the oscilloscope.

Thus, the research question for this paper goes: “Is it possible to use aliasing for measuring frequencies above the sampling frequency of a low-end oscilloscope with the help of low- and band-pass filters?”

For prototyping this approach an analysis is made in section II

on what is required and what kind of filter is needed to achieve the set goals. Utilizing this knowledge in section III the design is realized. Subsequently simulations on the realistic design are performed in section IV for initial tests on the filter structure, followed by results in section V and a discussion of the results in section VI. Finally, at the end of the paper, a conclusion is drawn on the discussed results in section VII.

II. Filter Design

A. Filter Structure

From fig. 1, the frequency and magnitude response of a low-end oscilloscope can be seen. This oscilloscope has a 20MHz bandwidth and a triangular filter response. What can be noted too, is that as frequency increases, the attenuation of the input signal increases. To prioritize the evaluation of the new approach rather than assessing the oscilloscope's dynamic range and upper-frequency limit for reliable frequency measurements, the introduction of a simple parallel filter structure is proposed, consisting of only a few filters. The proposed structure incorporates 3 filters; a low-pass filter with a pass-band of 0-20MHz, a first band-pass filter with a pass-band of 20-40MHz, and a second band-pass filter with a pass-band of 40-60MHz. These filters will also be called accordingly. This structure is expected to be able to assess triple the bandwidth by combining analog filters with signal processing.
The proposed filters are thus far considered ideal, i.e. perfectly square filters without transition bandwidths, no ripple in the pass-band, and an infinitely deep stop-band floor. In reality, however, perfectly square band-pass filters are not feasible. A trade-off has to be made between transition bandwidth, pass- & stop-band ripple, and stop-band attenuation.

B. Transition Bandwidth and Filter Order

Firstly, as a transition bandwidth is unavoidable, difficulties appear. In this area, namely, two different frequencies can occupy one frequency in the original bandwidth of the oscilloscope. Preventing this ambiguity, however, is still feasible with some conditions. This can be done by evaluating the magnitude response of multiple filters simultaneously.
When a mono-frequency signal, i.e. a signal with only one

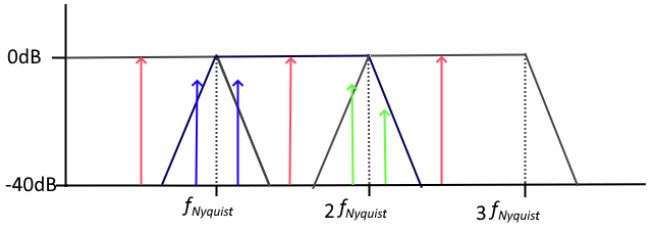

Fig. 2. Filter design with transition bands. Frequency components indicated by colored arrows with different evaluations, which fall in the transition band too

significant frequency included, with unknown magnitude is present at the edge of the pass-band of one filter, it can also be measured by the transition bandwidth of another filter. An illustration of this is given in fig. 2. Both the low-pass as well as the first band-pass filter detect a frequency and the same can be said for the two bandpass filters. However, these frequencies will be attenuated by different amounts. This indicates that the frequency lies in the transition region between the two filter frequencies. By analyzing the relative signal strength of both systems, it becomes possible to determine the actually received frequency, as this is the frequency with the largest relative magnitude.
On the other hand, if a signal with more than one frequency component is received, problems can arrive. This happens when two frequencies, which are at an equal distance from a multiple of the Nyquist frequency/a folding point, are received on one frequency in the baseband of the oscilloscope.
Still, it is possible to detect two frequencies in case the magnitude of the frequency components and the magnitude response of the filters is known.
While frequency A with magnitude A is in the pass-band of a filter, frequency B with magnitude B is in the transition band of the same filter at the other side of the folding point with equal distance. Frequency B, however, is attenuated by the transition band while frequency A is not. When the output of the filter is evaluated, it can be seen that a higher magnitude is measured for the frequency in the baseband than the magnitude of frequency A. This means that another frequency, in this case frequency B, was folded onto frequency A. The same can be said for frequency B in the pass-band and frequency A in the transition band.
Following this, to keep the frequency range for measuring multi-frequency signals with an unknown magnitude as great as possible, a small transition bandwidth is required. However, to decrease the transition bandwidth, filters of higher order are required which also require more filter stages. To maintain a feasible design, a maximum filter order of 10 was set. This should limit the number of components and thus parasitics. From this follows that the transition band for the low-pass filter and the left cut-off of the first band-pass filter are around 1MHz(5% of the pass-band) and a transition band of around 1.5MHz(7.5% of the pass-band) for the right side of the pass-band of the first band-pass filter and the left side of the second band-pass filter. With this approach, at least 87.5% of the pass-bands of all filters can be used with full certainty if the signal is multi-frequency and 100% if it is a mono-frequency signal. Note that, to achieve this, signal processing is required. This, however, will further be explained, after deciding on the filter type.

1) Ripple: A second requirement, on attenuation of the stop-band relative to the pass-band, is set at minimally 40dB. With such attenuation, frequencies in the pass-band are well into another order of magnitude than frequencies falling in the stop-band, ensuring clarity on what frequency was actually passed and which frequency was not.
Also, it is desired that the original signal is not affected in magnitude heavily by the filter in the pass-band. Therefore ripple in the pass-band is limited to 0.1dB and the ripple in the stop-band is not of any concern as long as it remains limited to maximally -40 dB.

2) Functionality: A simple and easily understandable design is desired which is easy to produce and repairable due to

the time limitations of this project. In addition, the device is required to triple the original bandwidth as was stated earlier and should be able to operate at a low-end oscilloscope with an impedance of $1M\Omega$.

C. Filter Choice

Now that the filter requirements are clear, a suitable filter needs to be found. Many filter types exist, which can generally be subdivided into passive and active filters. Passive filters can vary from filters such as sound acoustic wave [4] filters or MEMS filters [5] to LC filters. Generally, MEMS and SAW filters are very intricate to construct and more complex to design and repair due to their size. Furthermore, many active filter designs were researched and made in the past, often based on transistors. These filters are generally able to operate well at a few GHz, making these very interesting for high-frequency applications.
Ordinary LC filters, however, are of the highest interest, as these are relatively simple to design and are able to satisfy the requirements.
Ordinary LC filters have low noise compared to their active counterparts, have no power usage except for component loss, are unconditionally stable, are fairly insensitive to component variation, and do not require any biasing. On the other hand, inductors tend to be relatively large and do not function well at frequencies from 1GHz onwards [6]. However, as for this design, only filters are needed that need to pass frequencies until 60MHz with a very low priority for miniaturization. Therefore, large air-core inductors can be used, which generally provide a Quality-factor(Q-factor) [7] [8] of around 50 from 10MHz onwards, which is expected to be sufficient but will be verified in section IV.

D. Filter Topology

A topology needs to be chosen for the LC filter. Therefore a comparison is made on the requirements which can be seen in fig. 3. From this fig. 3, it can be observed that the elliptic

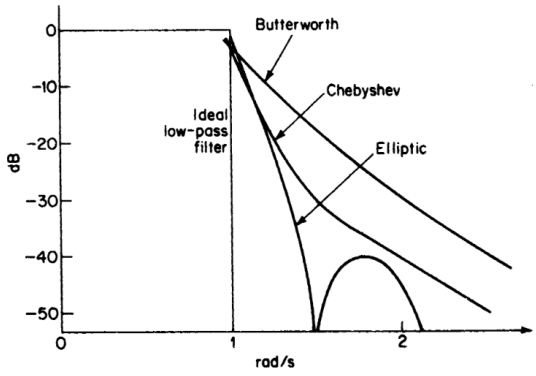

Fig. 3. LC filter roll-off comparison(Chebyshev II and Elliptic filter 0.1dB ripple pass-band) [9]

filter has the maximum roll-off for the Nth order and that pass-band ripple can be contained to 0.1dB simultaneously. For this reason, the elliptic filter is chosen.

E. Filter Order

Now that it is clear that elliptic LC filters will be used, a design can be made. This design can be made based on the parameters set previously, which can also be seen in table I. Using the requirements from table I, the filter order can be calculated using eq. (2-8) [10]. First an equation is used for taking into account the maximum allowed ripple as can be seen in eq. (2).

TABLE I
SUMMARY OF PARAMETER REQUIREMENTS OF A FILTER IN PROPOSED DESIGN

Parameter	Required
Stopband attenuation	>40dB
Passband ripple	<1dB
Transition Bandwidth	1MHz; 1.5MHz

$$\eta = \frac{10^{0.1A_\mathrm{s}} - 1}{10^{0.1A_\mathrm{p}} - 1} \tag{2}$$

for which A_s maximum stopband loss and A_p maximum passband loss. After the ripple is taken into account for determining the filter order, a parameter u can be calculated as can be seen in eq. (3) which will be used later.

$$u(\eta) = \frac{1}{16\eta}(1 + \frac{1}{2\eta}) \tag{3}$$

Furthermore, the cut-off frequencies for the pass- & stop-band are taken into account. This is done in eq. 4.

$$v(\omega_\mathrm{s}) = \frac{\sqrt{\omega_\mathrm{s}} - 1}{2(\sqrt{\omega_\mathrm{s}} + 1)} \tag{4}$$

of which eq. 5 for the low-pass filter will be used:

$$\omega_\mathrm{s} = \frac{f_\mathrm{s}}{f_\mathrm{p}} \tag{5}$$

for which f_s the frequency where magnitude reaches stop-band and f_p the frequency where the magnitude reaches the pass-band.
For the band-pass filters eq. 6 is used.

$$\omega_\mathrm{s} = \frac{f_{\mathrm{s}2} - f_{\mathrm{s}1}}{f_{\mathrm{p}2} - f_{\mathrm{p}1}} \tag{6}$$

for which $f_{\mathrm{s}1}$ and $f_{\mathrm{s}2}$ $f_{\mathrm{p}1}$ and $f_{\mathrm{p}2}$ are the frequencies where the magnitude reaches stop- and pass-band at the left and right edge respectively. Using the results of u and v we can calculate the order which is given by

$$n = F(u)F(v) \tag{7}$$

where

$$F(x) = \frac{1}{\pi} ln(x + 2x^5 + 15x^9) \tag{8}$$

Inserting the requirements, the low-pass filter results to be of 9th order and both band-pass filters to be of 7th order.

III. Realisation of Filter Design

In this subsection, the design that was given shape in section II will be realized into a physical prototype. Also, the measurement setup will be described.

Firstly, a circuit needs to be created that exhibits the desired performance. Due to the high order and thus high complexity of the filters, the circuit was generated by the software of Agilent [11]. The circuit that was generated with ideal components without parasitics is still to be converted to a non-ideal version with parasitics and non-exact components. The schematic can be seen in fig. 4. It was chosen to design a printed circuit board (PCB) for this purpose, to minimize the trace length and the possibility of using surface-mounted device (SMD) components. This minimizes parasitics and would therefore be preferred rather than ordinary through-hole components [12]. Also, parasitic coupling between components and ground needs to be taken into account. It is important to note that inductors that are in close proximity are placed perpendicular to each other. This reduces the mutual inductance significantly. Furthermore, coupling to the ground can be taken into account for the inductors. This coupling, however, is relatively small compared to the effects of component tolerance 5% component tolerance [13]. The PCB design can be found in appendix A. Although impedance matching was taken into account for one filter connected to the oscilloscope at a time, it is still desired to test if the filters work in parallel. For this purpose, a slightly altered second design was proposed with a resistor of 50Ω between the input of a filter and the filter itself. This resistor will be called a coupling resistor.

Apart from general damping over the complete magnitude response and highly damped peaks in the magnitude response, the resistors should prevent a direct short to ground for the two filters that are stopping frequencies in the stop-band while the third filter desires to pass that same frequency. This direct short, namely, could cause a deficiency of current for the third filter to induce enough voltage on the load of the oscilloscope. It was also chosen to use a 50Ω resistor, as this may maintain the impedance matching of a 50Ω in- and output

For performing measurements without the resistors, the resistors can be removed and substituted with some conducting material which will function as a short.

1) Measurement Set-up: For taking measurements, on the PCB 3 50Ω BNC in- and outputs were added. To the inputs, a wave generator is added while at the output a high-end and a low-end oscilloscope can be connected. To test these filters individually, one can simply connect the wave generator to the input of a filter of choice while the same can be done for the output. When a simultaneous filter measurement is desired, one splits the signal from the wave generator into 3 parts and inputs these separately to the filters. The outputs can be read out individually again.

IV. Simulation

With simulations, an expectation can be set on the performance of the design. The simulations in this section are only carried out on the proposed design analyzed in section II This means that the filter structures with a coupling resistor and/or are connected simultaneously are omitted, as no proper analysis has been executed on these and therefore nothing can be verified. A simulation on an ideal system will be carried out first, subsequently, simulations will be performed on the less ideal system.

1) Ideal system: A complete ideal system simulation on the magnitude with varying frequency was performed in LTSpice XIV which resulted in fig. 5. In this figure, the ripple is not noticeable and also turns out to be exactly 0.1dB. Furthermore, the stopband remains under -40dB, and also the transition bands are around the expected 1MHz and 1.5MHz respectively.

2) Nonideal systems: A complete non-ideal system simulation was also performed. In this model, non-ideal valued components with 5% tolerance with inductors of 0.2Ω internal resistance were incorporated as well as parasitics. As a rule of thumb, 1nH per millimeter trace was added and parasitic capacitance was neglected, since the parasitic capacitance per mm would only be in the range of maximally a few pF [14], which was not considered significant. For this non-ideal system, the result can be seen in fig.6. What can be noted is that due to the approximation of component values and the addition of parasitics, the magnitude response of the filters changed. The maximum ripple in the pass-band increased to approximately 6dB for all filters in the pass-band and also the stop- and cut-off frequencies were shifted. The transition bandwidths remained similar, except for the left edge of the second band-pass filter.

To observe the significance of component tolerance, a Monte Carlo simulation is performed on the proposed circuit, which can be viewed in figure 7 From this graph, a shift of around 1MHz can be expected for the cut-off frequencies of the realized non-ideal model's measurements.

V. Results

A. Magnitude Response of 4 filter structures

After having simulated the proposed design, measurements on the physical filters can be performed.

To commence the results section, the magnitude response of the filters will be measured. This was done for a frequency range of 0-70MHz to capture all 3 pass-bands and to validate if these filters show the expected behavior until 60MHz and are all stopping signals after 60MHz. In order to ensure the reliability of the magnitude response, a high-end oscilloscope was employed as the primary tool for obtaining accurate results.

A total of four types of filter measurements were conducted with this high-end oscilloscope. Firstly, each filter was individually connected to the oscilloscope's load and two measurements were taken for each filter. The first measurement was carried out with the coupling resistor, while the second measurement was performed without. Subsequently, two additional measurements were performed with all filters simultaneously connected to the oscilloscope's load.

After taking the magnitude response of the filters, also the magnitude response of the oscilloscope will be taken to correct for the attenuation caused by the oscilloscope without a filter

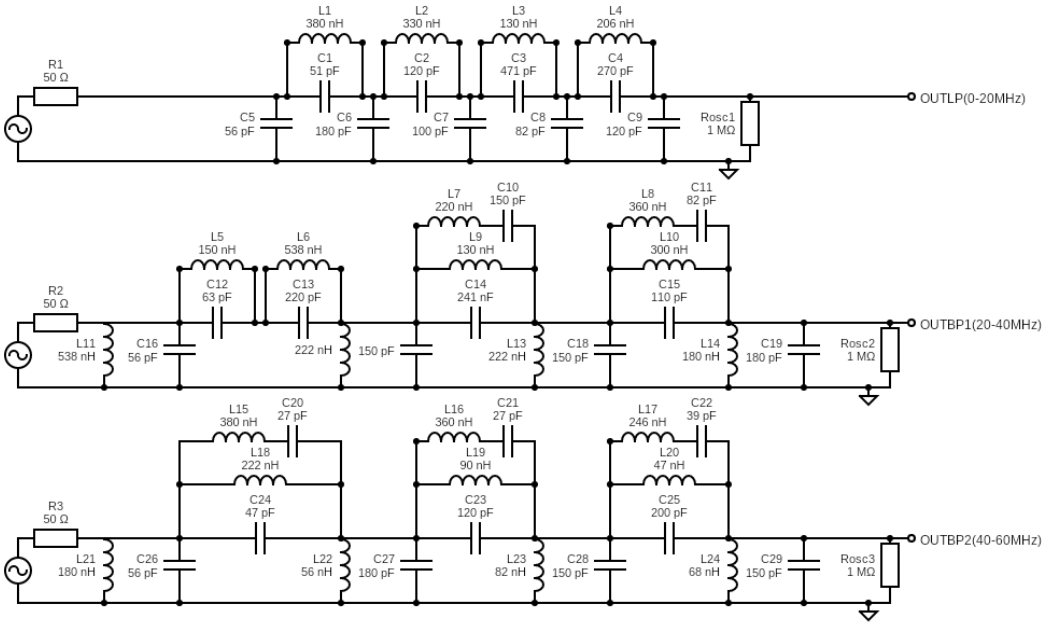

Fig. 4. Schematic of used filters, including sources and impedance oscilloscope($1M\Omega$)

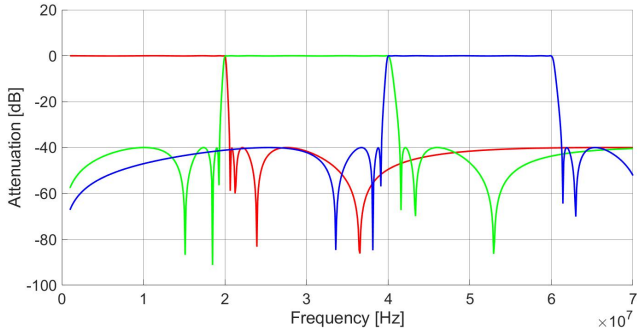

Fig. 5. Simulation of ideal filters

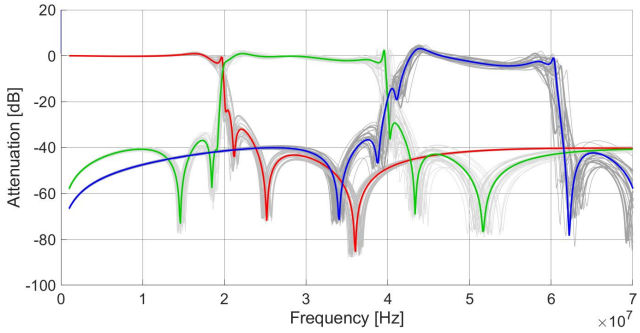

Fig. 7. Simulation of non-ideal system with monte carlo analysis

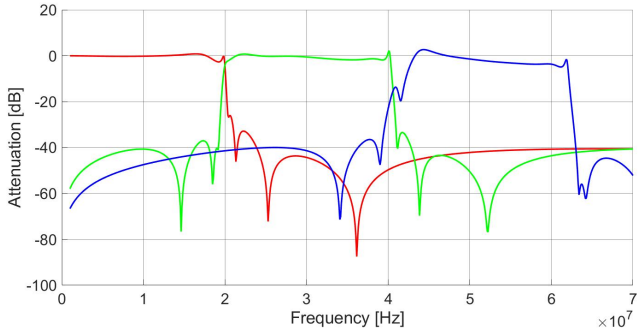

Fig. 6. Simulation of non-ideal filters.

between the wave generator and the oscilloscope. This way, the actual filter response can be acquired.
The approach with the results closest to the ideal filter magnitude response is measured again on the low-end oscilloscope, which results also will be corrected.

Finally, some measurements will be carried out with some individual signals.

1) Individually connected: In fig. 8 the response without a coupling resistor can be seen, while in fig. 9 the behavior with a coupling resistor is shown For the first filter structure in fig. 8, it can be seen that the measured response approximates the simulated response in the stop-band for all three filters. Some peaks are visible that exceed the minimum stop-band attenuation until -30dB or -20dB. This, most notably, happens for the second band-pass filter at 38MHz, the first band-pass filter at 45MHz, and for the low-pass filter at 50MHz. For the pass-band, there are also multiple differences compared to the simulation. Firstly, the cut-off of the low-pass filter is less steep. Secondly, the right edge of the pass-band of the first pass-band filter and the right edge of the pass-band of the second band-pass filter is also too early. These shifts, however, are in the range of 1MHz and 1.5MHz respectively as described in IV and thus could be expected.

For the second filter structure, with a coupling resistor,

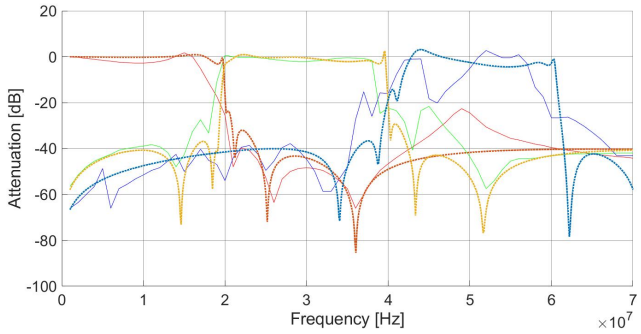

Fig. 8. Magnitude response of filter structure: simulation (dotted line) vs. measurement (solid line) with filters connected to the oscilloscope individually

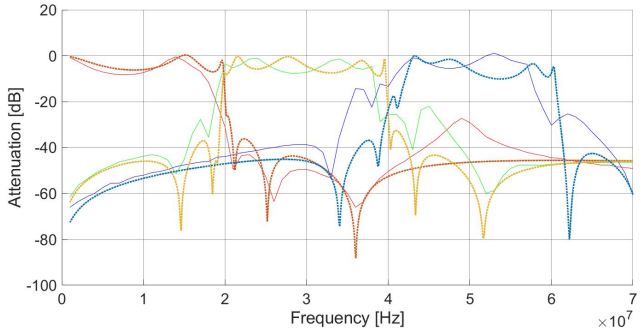

Fig. 9. Magnitude response of resistor-coupled filter structure: simulation (dotted line) vs. measurement (solid line) with filters connected to the oscilloscope individually

measurements were performed as well. Similarly, like for the second filter structure, fig. 9 demonstrates a relatively accurate tracking of the simulated response in the stop-band except for peaks at the same places as described for the filter structure without a coupling resistor. In general, it can be seen that the measured ripple increased to approximately $\pm 10dB$, as was expected by the simulation. The measured ripple does not, however, track the expected pass-band ripple.

2) Simultaneously connected: Now, the filter structure will be simultaneously connected to the oscilloscope.

Upon examining fig. 10, a very different response is measured

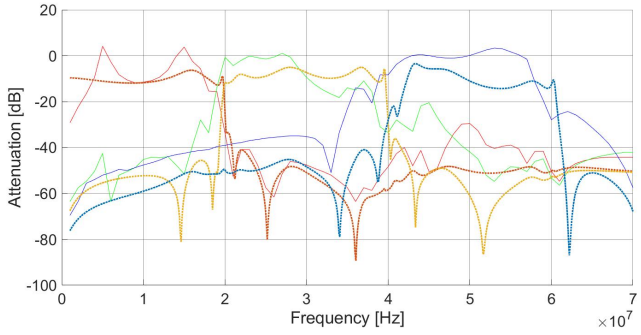

Fig. 10. Magnitude response of filter structure: simulation (dotted line) vs. measurement (solid line) with all filters connected to the oscilloscope simultaneously

than what was expected by simulation. Like for the individually connected filters, also these filters have cut-off frequencies and stop-band peaks at the places described previously for the filter without a coupling resistor. However, a notable difference in measured magnitude response can be observed in the pass-band of all three filters compared to the simulation. The low-pass filter peaks instead of staying at a relatively straight pass-band as well as the pass-band of the first band-pass filter which starts off higher than expected and finishes lower.

In figure 11 less difference can be observed between the

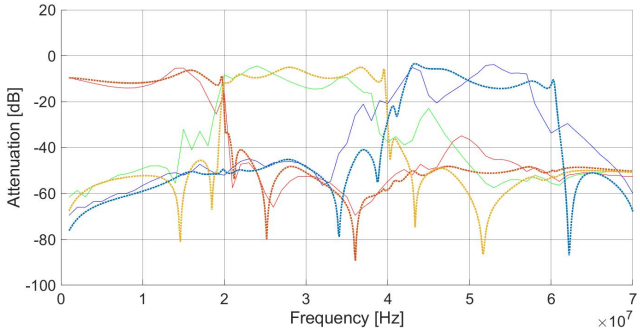

Fig. 11. Magnitude response of resistor-coupled filter structure: simulation (dotted line) vs. measurement (solid line) with all filters connected to the oscilloscope simultaneously

expected and measured pass-band. An attenuation of -10dB can be observed for all filters, however. The behavior of the stop-band is followed approximately well. The cut-off frequencies, however, are shifted slightly in the same fashion as happened for the other filters as well as the same stop-band peaks that can be observed. Finally, the first band-pass filter in particular has shifted ripple in the pass-band. The pass-band of the second band-pass filter is even more affected, with a significantly less steep transition band.

B. Low-end oscilloscope Response

As the filter without a coupling resistor and individual measurements of the filters resulted in the filter performance closest to the desired performance of a low amount of ripple and a stop-band at -40dB, a choice was made to continue measurements on the low-end oscilloscope with only this filter structure.

From this filter structure a magnitude response and a frequency response were retrieved by using the low-end oscilloscope and a comparison was made between inputting the signal with and without the filter.

Generally, the filters exhibit the same behavior as expected compared to the simulation and a significantly different behavior compared to the oscilloscope. However, the same shifts in cut-off can be observed as mentioned previously. Also, the stop-band of the filters exceeds the minimum attenuation of 40dB slightly, most significantly at 35MHz for the second band-pass filter. However, stop-band performance improved compared to fig. 8.

The folding behavior has not changed compared to the behavior without a filter, as was seen in fig.1.

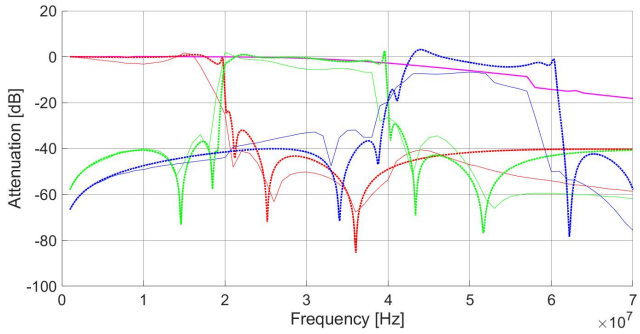

Fig. 12. Magnitude response in simulation(dotted line) and measured(solid line) result of filter with magenta line magnitude response of low-end oscilloscope without filter structure

TABLE II
ATTENUATION OF SIGNALS

Frequency[MHz]	$\text{Signal}_{\text{mono-frequency}}$[dB]	$\text{Signal}_{\text{multi-frequency}}$[dB]
19.5	-27.7	-27.2
20.5	-6.8	-2.2 - -5.2
39.5	-43.2	-36.2 - -55.2
40.5	-25.5	-28.2

C. Individual Signals

As the magnitude response of the first prototype has been measured, measurements can be done with different kinds of signals. The signals that will be tested will be at the same positions as the signals that were shown in fig. 2. These allow for testing a broad spectrum of signals, as with this frequencies outside the transition are tested, frequencies that occur at one distance from the folding frequency, and for frequencies that occur at equal distance from the folding point.

1) Frequencies outside the Transition Band: First of all, the passband without transition bands was desired to be tested. This was done by inserting 3 signals individually: 10MHz, 30MHz and 50MHz. These were inputted through the filters to the low-end oscilloscope and were received with at minimum -6.7dB in the passband of the dedicated filter and was stopped by maximally -33dB, which can be considered as a significant difference. Similar results can be expected for other signals with frequencies outside the transition band, thus resulting in no ambiguity.

2) Frequencies inside the Transition Band: To verify if the behavior of the filter structure can actually be used in the transition band, sample signals with equal magnitude are inserted through the filter into the low-end oscilloscope. Firstly, the frequencies 19.5MHz, 20.5Mhz, 39.5Mhz, and 40.5 MHz were inserted, where after these were measured by the filter with the corresponding intended bandwidth(19.5MHz by the low-pass filter, 20.5MHZ and 29.5MHz by first band-pass filter, and 40.5MHz by the second band-pass filter). After this, the frequency at the other side of the folding point was added to observe the significance of the frequency from the transition band falling onto the frequency in the passband. The results can be seen in table II. These are not corrected for attenuation of the low-end oscilloscope itself. With the measurements from table II several observations can be done. First of all, it can be noted that the signal strength is not around 0dB for all signals due to the attenuation which was also observed in fig. 12. For frequency detection of mono-frequency signals, however, some things can be said. As the attenuation levels of 19.5MHz and 20.5MHz are significantly different, it can be stated that these frequencies are not ambiguous in the case an equal magnitude frequency was to be measured at 19.5MHz, as 20.5MHz would fold to this frequency. The same can be said for 39.5MHz and 40.5MHz when a measurement is carried out at 500kHz, where these frequencies would fold to.
Now the mirroring frequency is added too, which allows for measurements on the determination of multi-frequency signals. A slight decrease in attenuation can be seen for the measurements with an input signal with frequency components at 19.5MHz and 20.5MHz. A frequency from the transition band folds onto the frequency in the pass-band. For 39.5MHz and 40.5MHz, however, the opposite is measured. It needs to be noted that the amplitude of 20.5MHz varies greatly as well as for 39.5MHz.

VI. DISCUSSION

Now that all simulations and measurements are finished, results can be discussed. Firstly, this is carried out for the magnitude response of the filters that were connected in different configurations. Then a comparison is made between the magnitude response of the chosen filter configuration and the low-end oscilloscope magnitude response. Finally, the mono- and multi-frequency measurements will be discussed.

A. Response of 4 measurement configurations

First, some general remarks can be made on these 4 measurements, after which differences between (non)-coupled and individually/simultaneously measured configurations are discussed.

1) General remarks on filter performance of all configurations: For all 4 cases, the cut-off frequency of the pass-band did not turn out as steep as expected. Generally, the cut-offs of the low-pass filter and the right edge of the second band-pass filter were less steep. This can be explained by the fact that all inductors were modeled with the same internal resistance of 0.2Ω. This resistance, however, was much higher for the low-pass filter, which follows from eq. 9 [15] for the Q-factor of the used inductors at frequencies between 0-20MHz [7], [8].

$$Q = \frac{2\pi f R}{L} \tag{9}$$

for which f the frequency R the internal inductance and L the inductance.
From this follows that for the used inductors the resistance of inductors in the low-pass filter at, for example, 20MHz is between $0.38 - 0.96\Omega$. Taking this into account in the simulation, performance already improves.
Furthermore, the other transition bands are shifted from the bands as expected from the simulation. It can be seen, however, that when the Monte Carlo simulation is observed, a shift of approximately 1MHz was expected for the first transition region edges and 1.5MHz for the second transition region

edges. This also partly explains many variations in ripple and in the pass- and stop-band that shifted peaks or degraded the attenuation up to -30dB or -20dB. This effect might have been strengthened by coupling of components to ground and other components [13].

2) Remarks on configurations: Some other remarks can be made between the four configurations. Firstly, a difference in ripple magnitude for the individually measured filters can be noticed. This ripple is most likely due to a mismatch in impedance matching. A mismatch in impedance matching causes reflections that could result in undesirable fluctuations in the magnitude response, which can also be noticed in the measurement for the resistor-coupled configuration. For the simultaneously measured filter structure, however, the non-resistor-coupled appears to show more fluctuation in the magnitude response. This can be explained due to the fact that the resistor-coupled simultaneously measured system has a general attenuation of -10dB which also damps the ripple. It seems like the voltage is attenuated by exactly $-10dB \approx \frac{1}{3}$, which seems an equal division over the three filters. This is discussable as the impedance of the three filters should not be equal at all times.
In addition, It is also expected that the coupling resistance damped peaks both up and down of the magnitude response, unlike for the configuration without a coupling resistance.

B. Low-End Oscilloscope Response

The magnitude response is very similar to the expected response. Once more the effect of a too-low internal resistance for the low-pass filter can be observed, as well as shifted transition bands. The pass-band of the second band-pass filter is lower than expected and in general a downward trend can be observed in the pass-bands of the filters, despite a correction for this filter was made with regards to the magnitude response of the oscilloscope itself. This can possibly be explained by an increased loss inside the circuitry at higher frequencies.
Compared to the response of the oscilloscope without a filter, a significant change was made in implementing the new approach.

C. Mono- and Multi-frequency signals

Although the magnitude response of the filter structure is not ideal, still frequencies outside the transition bands were well definable.
For frequencies in the transition area, it also turned out possible to measure mono-frequency signals with significant differences if the magnitude of input is known. A test for unknown magnitudes could have been performed too. This could have been done by measuring all mono-frequency signals separately by the other filters, whereafter a comparison could be made in the magnitude of the intended passing filter and the filters intended in the stop-band. This would most likely have resulted in a relatively smaller attenuation for the signal in the pass-band, which would have proven the analysis in section II
. For multi-frequency signals also a measurement was performed on allowing opposite frequencies with an equal magnitude of equal distance from the folding point to fold into one frequency. This resulted in even less attenuated signals compared to mono-frequency signals. From this can be concluded that another frequency must have folded on this frequency in the baseband. This, however, is not a very significant difference at 19.5MHz, which makes determining the frequency less reliable. In addition, this difference varies for 20.5MHz and 39.5MHz, which can be explained due to jitter in the sampler which could shift folded frequencies just past the expected peak. At 40.5MHz, even an increase of attenuation is measured. This could possibly be due to destructive interference, this is, however, debatable, as the same effect was directly seen for the other frequencies.
In addition, it must be noted that with an unknown magnitude of the frequencies still approach is impossible.

VII. Conclusion

A new approach for increasing the bandwidth of a low-end oscilloscope has been developed. Folded frequencies can be considered unambiguous in areas without the transition bands of filters. In areas with transition bands, however, it turns out that magnitude and filter magnitude response is required to know what frequency exactly is detected for a multi-frequency signal, but that this is not always required for a mono-frequency signal. These signals, namely, can be determined if there is a largest relative magnitude between the outputs of two filters.

VIII. Future Work

In future work, it can be further investigated whether at higher frequency ranges the proposed design still functions. Furthermore, more research is possible if the inductors used could be made smaller or replaced by smaller component(s) with an equivalent functioning for miniaturization.

References

[1] Derek E Toeppen. Acquisition clock dithering in a digital oscilloscope. *Hewlett-Packward J*, 48(2), 1949.

[2] J. Baier and H.W. Furst. A novel method for detection of aliased frequency components in fft-based spectrum analysers and digital oscilloscopes. In *1993 IEEE International Symposium on Circuits and Systems*, pages 770–773 vol.1, 1993.

[3] Patrick Koch and Niek Moonen. Investigation of anti-aliasing filter performance in low-end oscilloscopes. In *2023 IEEE 7th Global Electromagnetic Compatibility Conference (GEMCCON)*, pages 6–7, 2023.

[4] R. Weigel, K. Weigenthaler, R. Dill, and I. Schropp. A 900 mhz ladder-type saw filter duplexer. In *1996 IEEE MTT-S International Microwave Symposium Digest*, volume 2, pages 413–416 vol.2, 1996.

[5] Keiichi Motoi, Naoki Oshima, Masaki Kitsunezuka, and Kazuaki Kunihiro. A band-switchable and tunable nested bandpass filter with continuous 0.4–3ghz coverage. In *2016 11th European Microwave Integrated Circuits Conference (EuMIC)*, pages 492–495, 2016.

[6] George S. Moschytz. *Analog Circuit Theory and Filter Design in the Digital World*. Springer International Publishing, 2019.

[7] Coilcraft. *Maxi Spring™ Air Core Inductors*, 12 2021.

[8] Coilcraft. *Square Air Core Inductors*, 12 2021.

[9] Arthur B. Williams and Fred J. Taylor. *Electronic Filter Design Handbook*. McGraw-Hill, fourth edition, 2006.

[10] R Raut and M N S Swamy. *Modern analog filter analysis and design*. Wiley-VCH Verlag, Weinheim, Germany, October 2010.

[11] Keysight. Pathwave advanced design system (ads) bundles, Oct 2020.

[12] Cleyton R. Paul. pages 315, 759. Wiley-interscience, second edition, 2006.

[13] Shuo Wang, F.C. Lee, D.Y. Chen, and W.G. Odendaal. Effects of parasitic parameters on emi filter performance. In *IEEE 34th Annual Conference on Power Electronics Specialist, 2003. PESC '03.*, volume 1, pages 73–78 vol.1, 2003.

[14] James Karki. *Effect of Parasitic Capacitance in Op Amp Circuits*. Texas Instruments, Post Office Box 655303 Dallas, Texas 75265, September 2000. SLOA013A.

[15] TDK. What is the q value of an inductor (a coil)?

APPENDIX A

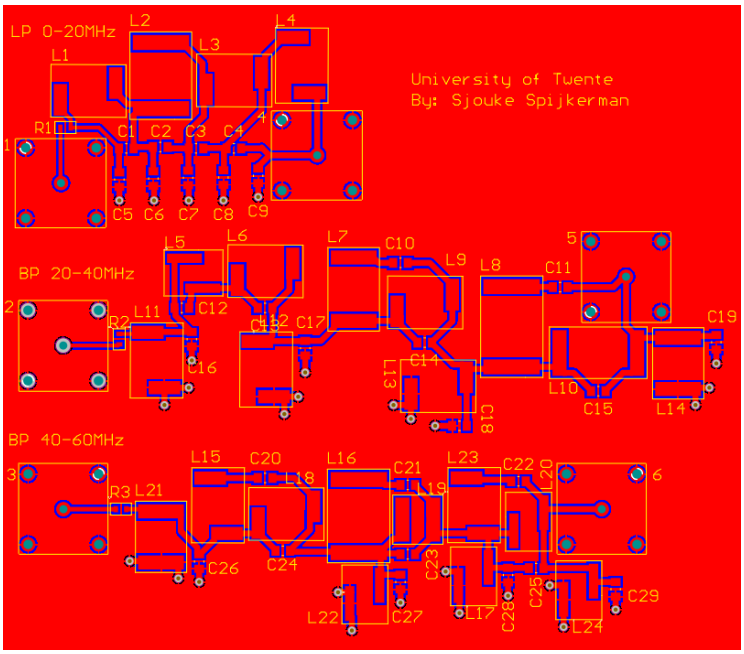

Fig. 13. PCB lay-out of schematic shown in fig. 4